A Regional Atmospheric Model in a Coastal Zone with Significant Wind and Wind Stress Curl: Comparison with Wind Station and Satellite Observations

Hsiao-ming Hsu[1], Lie-Yauw Oey[2+], Changming Dong[2], Clive Dorman[3] and Richard Hodur[4]

[1]National Center for Atmospheric Research[*]
Boulder, Colorado USA

[2]Princeton University
Princeton, New Jersey USA

[3]Scripps Institute of Oceanography
La Jolla, California, USA

[4]Naval Research Laboratory
Monterey, California, USA

December, 2002

[+] Corresponding Author: lyo@princeton.edu

[*] The National Center for Atmospheric Research is sponsored by the National Science Foundation.

ABSTRACT

Recent research has shown the sensitivity of simulated ocean currents to details of wind over the Santa Barbara Channel (SBC), California, a region with significant wind and wind stress curl. This study applies the Coupled Ocean/Atmosphere Mesoscale Prediction System (COAMPS) in a triple nesting configuration with 3:1 grid ratio (Δ = 81:27:9 km) centered over the SBC to examine the regional winds. A spring-transition period, March-May 1999, is chosen to evaluate and test the accuracy of COAMPS during these rather delicate months when wind changes from its characteristics more typical of winter (with storm passages) in early March, through April and May when multiple scales exist in the channel due to the existence of supercritical expansion fan and compression jump. The simulated results were checked against wind station time-series in the vicinity of the channel, and against speeds obtained from Special Sensor Microwave/Imager (SSM/I); they are also compared with reanalysis obtained from the European Center for Medium Range Weather Forecast (ECMWF).

It is found that COAMPS gives an overall large-scale structure comparable to that observed in climatology and previous model simulations: including expansion fans downwind of major Capes where speed increases and, in particular, onshore wind turning in the Southern California Bight (SCB), where southward along the coast both wind and wind stress curl weaken. The simulation indicates that this turning is the accumulated effect of synoptic-scale cyclonic eddies shed downwind of Pt. Conception during periods of intense equatorward wind in the open ocean. The turning (and eddies) are missing from the ECMWF reanalysis. The open-ocean COAMPS wind speeds agree with both SSM/I and ECMWF. In the SBC, while zones of small-scale (tens of km) vorticity structures and March-April variability are reasonably reproduced (as checked against wind station data), the model fails to correctly simulate the location and intensity of the expansion fan and compression jump in the channel during April-May transition. The

consequence is a spatially more coherent wind field along the channel, contrary to observed. There is indication that increasing the grid-resolution may improve the results.

1. INTRODUCTION

Wind stress is an important driving mechanism for coastal ocean circulations along much of the U.S. west coast (e.g. Allen, 1980). This includes the Central California Shelf and Slope (CCSS) and Southern California Bight (SCB), and the transition zone in between - the Santa Barbara Channel (SBC; Figure 1), where moreover effects of wind stress curl are also important (Oey, 1996, 1999, 2000; Munchow, 2000). However, with a few exceptions involving aircraft measurements during limited time periods (Brink and Muench, 1986; Caldwell et al. 1986), estimates of wind stress and wind stress curl over the CCSS-SBC-SCB coastal zone have been based on relatively sparse buoy and land-based measurements (Dorman and Winant, 1995, 2000). A comprehensive, high-resolution wind field is needed to characterize oceanographically relevant aspects of meteorological variability in the region. This paper attempts to address this issue.

Notable characteristics of mean winds over CCSS-SBC-SCB are that they are strong and persistently equatorward west of the channel and over the CCSS, and weak east of the channel and over the SCB. This can be seen in Figure 2, which shows the spring mean wind stress over the region computed from the California Cooperative Oceanic Fisheries Investigation (CalCOFI) observations. Mean wind stresses west of SBC and over the CCSS exceed 0.1 N m^{-2}, whereas east of SBC and near the coast in the SCB values become insignificant. The wind also contains short-time fluctuations, from diurnal to synoptic (days). The south/southeastward wind at the western entrance of SBC, for example, can reach 0.2-0.3 N m^{-2} (Dorman and Winant, 2000), and it decreases rapidly eastward over a distance of about 50km. This rapid eastward weakening is due primarily to blockage of winds from the north by mountain range along the channel's northern coast. The resulting wind stress curl is often in excess of 0.1 N m^{-2} per 100km (Munchow, 2000). These winds and wind stress curls are important driving agents of the regional ocean currents (Oey, 1996, 1999, 2000; Wang, 1997; Harms and Winant, 1998; Oey et al. 2001). Figure 3a, taken from Oey (2000), shows the sensitivity of the modeled ocean fields to detailed wind structures in the Santa Barbara Channel. The left panel shows modeled near-surface temperature and velocity fields when the ECMWF wind supplemented by over-ocean buoy wind data is used as forcing, and the right panel when additional land and island wind stations are also utilized. While the resulting winds in both cases look similar (Figure 3b), the wind stress curls are quite different. The solution forced by the more detailed wind field (Figure 3a, right panel) shows stronger cyclone over the western channel, brought about by the spatial variations in the wind stress curls in conjunction with the channel's geometry (Oey, 2000).

Our ultimate goal is to accurately simulate ocean currents in the vicinity of the Santa Barbara Channel, for which accurate wind field is essential. In this paper, we describe our attempt in simulating the winds for a three-month period, March-May 1999, using the Coupled Ocean/Atmosphere Mesoscale Prediction System (COAMPS; Hodur, 1997) developed at Naval Research Laboratory, Monterey. This period is chosen to test the model's ability to simulate the so called "spring transition" during which more erratic winds due to (late) winter storm passages in March give way to, in May, a more typically summer-time intense and persistently equatorward wind west of the channel, and weak winds further east. This shift in the wind field has been shown to correspond also to a shift in the regional ocean dynamics (Oey et al. 2002). Coupled with complex orography, the simulation is a challenge to any model. The COAMPS experiment is described in section 2, and section 3 presents monthly and three-month averaged fields. In section 4 we compare the COAMPS results with detailed time series from wind station observations, satellite, and also from ECMWF analysis. Section 5 discusses results in the synoptic time scales. The paper concludes with a summary in section 6.

2. NUMERICAL MODEL AND EXPERIMENTAL DESIGN

COAMPS solves the fully compressible, non-hydrostatic equations on Arakawa C-grid, and uses the height-based terrain following vertical coordinate grid. It includes physical parameterizations of short- and long-wave radiation (Harshvardhan *et al.* 1987), cumulus convection (Kain and Fritsch, 1990), and subgrid-scale boundary layer processes using a level-2.5 turbulent kinetic energy scheme (Therry and LaCarrere, 1983). Following Rutledge and Hobbs (1983), explicit moist physics contains prognostic equations of water vapor, cloud water, rain water, cloud ice and snowflakes. COAMPS has been verified and tested elsewhere (Hodur

1997; Doyle, 1997; Thompson *et al.* 1997; Burk et al. 1999), and has been run operationally by the navy in several coastal areas of the globe to provide real-time forecasts. COAMPS has nested-grid capability and uses MVOI (multivariate optimum interpolation) analysis to map the observations to its grid. Details can be found in Hodur (1997).

COAMPS simulations require NOGAPS (Navy Operational Global Atmospheric Prediction System) outputs produced by FNMOC (Fleet Numerical Meteorology and Oceanography Center). The NOGAPS datasets with 1^{o} resolution are interpolated to the COAMPS domain grids as a first guess. The first guess fields are then further enhanced by available observations: radiosondes, surface stations and aircraft reports. Incremental assimilation is used every twelve hours to incorporate the observations.

The model topography is derived from the Defense Mapping Agency's 100-m resolution dataset sub-sampled to 1-km resolution, while sea surface temperature (SST) is obtained by a bilinear interpolation of the FNMOC global 1^{o} SST optimum interpolation analysis to the COAMPS domains.

A triply nested domain is configured with one-way interaction between the outer domain (59 × 59 grid points), the middle domain (61 × 61 grid points), and the inner domain (91 × 91 grid points) centered over the Santa Barbara Channel (Figure 4). The horizontal resolutions are 81, 27, and 9 km for the three grids, respectively. The model top is 31 km and there are 30 unevenly spaced vertical sigma levels, with 11 levels in the lowest 1.6 km, down to 10 m for the grid nearest the ocean surface. The Kain-Fritsch cumulus parameterization is used only on the two outer nests. The NOGAPS dataset are made available to us every 12 hours during the three-month simulation period, March – May, 1999.

3. MODEL RESULTS

In view of our focus on utilizing the wind as forcing on the ocean currents, we will examine only the near-surface field, i.e. winds at the lowest sigma level at 10 m above the ocean.

A detailed description of the model structure of the lower atmosphere will be the subject of a separate paper. In the followings, this 10-m wind will simply be referred to as the "wind." The winds are converted into wind stresses using the Large and Pond's (1981) bulk formula assuming neutral stability. The assumption is reasonable in view of the relatively small air-sea temperature difference in the region (Dorman and Winant, 2000). We will first discuss the three-month averaged fields, then the monthly and shorter time-scale results.

Three-Month, March-May Averages

Figure 5 shows contours of (a) wind speed, (b) wind stress, (c) wind stress curl and (d) divergence averaged over March through May 1999. These were derived from the inner-nest domain. (For more clarity in the region of interest, the plotted domain is approximately 150 km smaller on all four sides). Surface streamlines indicating flow directions are superimposed on each panel, but over-land contours are omitted in order to emphasize the over-ocean fields. The mean wind off the central and northern California coast is north-northwesterly almost parallel to the coastline, with speeds generally greater than 6 m s^{-1} and corresponding wind stress > 1 dyne cm^{-2}. These rapidly decrease near the coast within a cross-shore width of about 50~100 km. The speed is generally weak ≈ 1-2 m s^{-1} over land (not shown). Inside and south of SBC in the SCB, the wind veers cyclonically and also weakens. In the Bight, wind is from the west blowing almost in an onshore direction, with weak speeds 1~2 m s^{-1}, and stresses less than 0.2 dyne cm^{-2}. These features and values generally agree with the observation off central California and in SCB (Figure 2). The broad positive curl over the SCB is in part due to cyclonic eddies which, under proper synoptic conditions, can form in the lee of the mountains along the northern coast of the SBC (please see section 5). The stronger upwelling-favorable wind stress off the central and northern California coast is well-known to produce generally equatorward current and cool waters near coast (e.g. Beardsley and Lentz, 1987). On the contrary, upwelling is less marked in the southern California Bight (Harms and Winant, 1998).

The inner-nest domain shown in Figure 5 encompasses two Cape regions, Pt. Sur (36.3^{o}N, Monterey, just south of San Francisco) and Pt. Conception (34.4^{o}N), downwind of which the flow accelerates and mean speeds maximize to 6~7 m s^{-1}. These maxima in the lee of major capes, and minima upstream, have been described by Korachin and Dorman (2001). These authors also show (from their MM5 model) that the maxima generally coincide with (surface) flow divergence while upstream and immediately in the lee of the Cape near the coast is convergence. COMAPS divergence field in Figure 5d shows similar features. The wind stress curls also maximize downstream of these capes, reaching high values of ≈ 0.3-0.5 N m^{-2} per 100 km. Note that in the Santa Barbara Channel, the curl is strongest and cyclonic in the northern half of the channel, and it changes sign to become anticyclonic, though much weakened, in the southern half. This detailed wind stress curl distribution arises because the (generally southeastward) wind maximizes near the channel's center consistent with observations (Dorman and Winant, 2000; please also see below). There is some evidence that the strong cyclonic curl in the channel is in part responsible for the spin-up of a cyclone in the ocean in the western portion of the channel especially in spring (Oey, 1999, 2000; Munchow, 2000; Oey et al. 2002). It is also interesting to note the strong cyclonic curl south of the channel islands – south of San Miguel and Santa Rosa in particular. On a larger scale, along the coast beginning from Pt. Conception south into the southern California Bight, the cyclonic wind stress curl continuously weakens to about 32^{o}N. This equatorward weakening has been shown to be important forcing that in part determines the along-coast ocean currents (Oey, 1996, 1999).

It is of interest to compare Figure 5 with the corresponding fields computed from the coarser-grid (27 km) middle-nest domain winds. Figure 6 shows these latter results. As can be expected, the coarser-grid winds are generally smoother, and features such as flow accelerations downstream of Pt. Sur and Pt. Conception appear less abrupt, with correspondingly weaker curls and divergences.

Monthly Variations

In term of the monthly mean fields, shown in Figure 7a for wind speeds, the strength of northwesterly surface flow increases from March to May, and indicates the eastward progression of the sub-tropical high over the eastern Pacific, coupled with development of low over the southwestern U.S. (Dorman and Winant, 2000). Accompanying this speed increase is the corresponding increase in wind stress curl (Figure 7b). These increases off central and northern California, and also over the western SBC, contribute to increased upwelling in the upper ocean in these regions, which normally occurs in April and May (Beardsley and Lentz, 1987; Harms and Winant, 1998). Moreover, since trapped waves propagate poleward, of importance to the coastal ocean response in the SBC and over the CCSS is also the wind off the southern California coast (Oey, 1996, 1999). Figure 7 shows subtle monthly changes in wind and wind stress curl in the eastern channel and near the coast in SCB. In these regions, both wind (speed) and wind stress curl are largest during April. This is related to transition of wind characteristic from winter to late spring and summer as will be described in more detail below in conjunction with observations. These subtle variations have important consequences to the ocean responses (Oey et al. 2002). Over the western channel, both wind (speed) and wind stress curl are largest in May. Indeed, the May values dominate in the three-month means shown earlier in Figure 5.

4. COMPARISON WITH WIND STATION DATA, SATELLITE AND ECMWF

Comparison with Wind Station Observations

We will make comparisons focusing in the Santa Barbara Channel region. The complexity of orography and dynamics (Dorman and Winant, 2000) in this region presents a challenge to any model. The period from about March through April off California coast is the so called "spring transition" during which the wind changes from a typical wintertime patterns frequented by passages of storms to a more organized and persistently stronger equatorward wind field over CCSS and western SBC, but weak winds over the SCB typical of the summer months (beginning in May). In the SBC, storms typically induce reversed, southeasterly (i.e. poleward) wind episodes (Dorman and Winant, 2000). Figure 8 plots the principal-axis (PA) winds observed (solid curves) at six stations 46023, 54, ROSA, 53, GAIL and 25 (for locations please see Figure 9 next).[1] The modeled winds (dashed curves for the middle-nest domain with $\Delta = 27$ km and dotted for the inner-nest domain with $\Delta = 9$ km) are also plotted. Figure 9 shows the observed and modeled PA wind ellipses at ten stations in the SBC region.[2] Positive PA is defined to be directed generally poleward for all stations. With curves generally below the zero-axis, Figure 8 therefore shows equatorward winds. However, at B23 and B54, two major reversed (i.e. poleward) wind episodes occur in March, on March/19th and 25th, with peaks ≈ 9 m/s and 6 m/s respectively at B23. The reversals extend to eastern and southern stations also, though weaker. These are followed by ten days of persistently strong equatorward wind (≈ 10 m/s at B23 and B54) from end of March through beginning of April. Through the rest of April, the strong equatorward wind is punctuated by a series of weakened or even slightly reversed wind events. Note that strong equatorward wind bursts occur more often from late March through April, than earlier times in March, and moreover they extend further to the southern and eastern stations (B53, GAIL and to a lesser degree B25). In May, the wind becomes more persistently equatorward during the first three weeks before it weakens near the end. In addition to the more persistent equatorward wind in May, Figure 8 also indicates a distinct change in fluctuations west and east of the Santa Barbara Channel in March/April and May. Winds are more coherent throughout the channel during March through April in that strong or weakened (and at times even reversed) equatorward winds in the west coincide with similar events in the east. Starting early May, the characteristics change quite abruptly (within one week) when winds in the east and southeast (in the southern California bight) weaken, while winds west and north intensify and become more persistently equatorward. This latter characteristic is typical of the summer-time winds (Dorman and Winant, 2000). The shift in (wind) behavior from spring-transition to summer is more clearly seen in plots of correlation coefficients between B54 and GAIL, and also between B54 and B53, as shown by the solid curves in Figure 10. (Modeled correlations, to be discussed shortly, are also plotted). The correlations are calculated using fifteen-day moving window, and the 95% significance curves are also plotted. The correlations between B54 and eastern stations are significant and relatively high (generally > 0.6) in March and April but drops below 0.4 and also the 95% significance curve in May. In terms of the ocean response, we show in Oey et al. (2002) that the strong equatorward wind bursts in early spring spanning the whole channel (late March through April, Figure 8) can account for the initiation of

---

[1] Reference to the NDBC stations will often be simply the last two digits preceded by "B;" e.g. B54 for 46054.

[2] We analyzed data at all the stations shown in Figure 1. Only ten focusing in the SBC region, as shown in Figure 9, are presented herein.

strong equatorward coastal currents off central California. Also, the May's weakened wind to east and south, coupled with persistent equatorward wind in the west, can set up along-channel pressure gradient necessary for the initiation of poleward coastal current along the northern coast of the channel (Oey, 1996, 1999; Oey et al. 2002).

The time-series comparison of Figure 8 shows that the model does well in reproducing the observed fluctuations in March and April, but rather poorly in May. The finer-grid ($\Delta = 9$ km) tends to give slightly better result, as can be seen also from the closer agreements (with observed) in the PA angles (see Figure 8). The proximity of the modeled values to those observed is summarized in Figure 11 in terms of model-observed correlation and skill "Sk" computed at all the ten stations. The skill is defined as:

$$\mathrm{Sk} = \{1 - <(\mathbf{u_m}-\mathbf{u_o})\bullet(\mathbf{u_m}-\mathbf{u_o})>/<\mathbf{u_o}\bullet\mathbf{u_o}>\},$$

where <.> is time averaging over the three-month period, '**u**' denotes wind vector, and subscripts 'm' and 'o' denote model and observation respectively (c.f. Davis, 1976). Values of Sk ≈ (but less than) 1 would in general indicate good agreements between model and observation. It is seen that both correlation and skill are quite high > 0.7, except at B53 and B25. The finer-grid gives generally better results, though only marginal, and at some stations it is actually worse (e.g. Sk at B53). Figure 8 indicates that the poor skill and correlation at B53 are because the model overestimates winds during May. (If May is excluded, the correlation and skill both increase to about 0.9. On the other hand, if May alone is used, the correlation drops to ≈ 0.4 and negative skill is obtained.) The overestimation of wind speed at B53 is because the modeled winds over the western and eastern portions of the channel are more correlated than they should be based on observations during May. Figure 10 shows this clearly. In fact, the modeled correlation curves are larger than those observed at all times. In other words, the modeled 'eddy' or spatial correlation scale is larger than observed. Dorman and Winant (2000) suggest that wind in the eastern channel zone is also affected by air flows from land. Moreover, supercritical expansion fan around Pt. Conception over the western channel exists, and this is followed by a hydraulic jump that occurs somewhere in the mid-channel. The jump occurs over distances of O(km)

(Dorman, 1985b; Winant et al., 1988; Samelson, 1992; Haack et al., 2001). Dynamically, the modeled wind in the east is predominantly part of the same Pacific pressure system as wind in the west. While this may be true in March and April, it no longer holds in May when observations show a distinct disconnect east and west (Figure 10). Figure 10 suggests that the results improve with higher grid resolution. However, even finer grid is necessary to resolve the detailed orography and simulate the correct location of the compression jump in the channel.

The PA-ellipse comparison in Figure 9 shows that in general the model underestimates variances. At the western and southern-channel stations (B23, B54, ROSA and CRUZ), the means are also underestimated, though they still exceed the variances as are also observed. At the northern-channel and eastern stations (HOND, B53, GAIL and B25), observed variances are larger than means, while the model shows means generally larger than variances. This discrepancy is related to the modeled correlation scale being larger than observed, especially during May, as explained in the previous paragraph.

Comparison with Satellite, Wind Station Observations, and with ECMWF Reanalysis

We now compare the inner-nest ($\Delta = 9$ km) COAMPS results with satellite and ECMWF products. The SSM/I (Special Sensor Microwave/Imager) data are produced as part of NASA's Pathfinder Program. A unified, physically based algorithm is used to simultaneously retrieve ocean wind speed (at 10 meters), water vapor, cloud water, and rain rate (Wentz, 1997; Wentz et al. 1998). Only the wind speed portion of the data is used for our purpose. (Note that the QuikScat product, which gives both wind speeds and directions, did not become available until July/1999). The three-day averaged fields on $1/4^{\circ}\times1/4^{\circ}$ grid were used to avoid prohibitively many missing data. These were further quality-controlled by flagging bad data at grid points where the speed and its spatial gradient exceed certain limits. (The data already comes with a near-coast strip of width ≈ 50-100 km flagged). The data were then checked against the ECMWF reanalysis product on 1.125° Gaussian grid by computing the correlation between the two speed products over the period from 1992 through 1999. The correlation was found to be significant and high (coefficients ≈ 0.8) over the open ocean, some 100 km off the coast (not shown). The speeds also agree well with available NDBC winds. The ECMWF u and v-winds were then checked by correlating them with available NDBC winds at *off-shore* locations. The correlations were also found to be high (coefficients ≈ 0.9), though the magnitudes were too low nearer the coast. Thus the ECMWF phasing is excellent while its magnitudes are too low near the coast. We therefore assume that the wind directions from ECMWF are correct at off-shore locations and replace its magnitudes by the SSM/I speeds. This latter product was then used in combination with all available near-coast wind stations data to optimally interpolate onto Oey et al.'s (2001) ocean domain (as shown by the rectangle in Figure 1) using 5 km × 5 km grid sizes. This final product is referred to as the SEN – Satellite-ECMWF-NDBC dataset. In addition to this product, Dr. Ed Dever (SIO) has also provided us with wind maps obtained by optimally-interpolating the coastal wind station data in the vicinity of the Santa Barbara Channel. This will be referred to as the SIO dataset.

Figure 12 compares the COAMPS, SIO, SEN and ECMWF mean wind stresses (March-May), Figure 13 the corresponding standard deviations, and Figure 14 the corresponding wind stress curls. Note that for SIO dataset an enlarged region telescoping on the channel region is shown. Over the open ocean, COAMPS winds compare quite well with SSM/I or SEN winds. In particular, both show a decrease along the ocean model's offshore boundary, by approximately the same amount of about 0.3 dyn/cm^2. The ECMWF wind also shows similar wind speeds, although the decrease is faster. Both ECMWF and SEN show little onshore turning south of Pt. Conception, while COAMPS is in better agreement in this regard with the observed climatological wind stress pattern shown in Figure 2. In the near-coast zone, a local maximum in wind stress at about the 36^{o}N latitude exists, corresponding to the expansion fan downwind of Pt. Sur as discussed previously. This feature agrees with SEN. On the other hand, the maximum just west of SBC, as seen both in SEN and SIO, is not simulated in COAMPS, which shifts the maximum further downwind south of the channel islands. As expected, the relatively coarse ECMWF wind field completely misses these fine-scale near-coast features. Similar conclusions are also seen in the standard-deviation plots (Figure 13): the strong variability in the western SBC as observed in SIO and SEN is missing from COAMPS and ECMWF. On the other hand, COAMPS' wind stress curl plot (Figure 14) shows reasonably realistic patterns of highs and lows particularly in SBC, where observed (from SIO and SEN) positive curl in the northern portion and negative curl in the southern portion of the channel are correctly simulated. Such features are missing in the COAMPS' coarser-resolution middle domain (Δ = 27 km; not shown but please see Figure 6c), as well as in ECMWF (Figure 14).

5. MESO-SCALE SYNOPTIC VARIABILITY

That coarse-grid ECMWF product does not show on-shore or eastward wind turning south of Pt. Conception (Figure 12) suggests that localized meso-scale eddies play a role in determining the mean field. In other words, the turning in the SCB (Figure 2) is not merely a large-scale feature derived from the Pacific. The COAMPS simulation (especially the finer inner-nest grid) provides examples on how eddy features can develop.

We find that the development of cyclonic eddy downwind of Pt. Conception is generally preceded by strong equatorward wind over the open ocean. The maximum speed often occurs just downwind of Pt. Conception over the western SBC. Figure 15 shows an example on May/16th (top-left panel) when the open-ocean speeds exceed 10 m s^{-1}. The four panels on the right show an example of cyclonic eddy development, 1~2 days after the intense wind, in terms of contours of vorticity on May/18th. In this case, the cyclone is sufficiently intense that the near-coast wind actually reverses at 13:00GMT. In the daily-averaged speed map (lower left panel), the effect shows up as a much weakened on-shore wind in the Southern California Bight. For the three-month simulation period, such "eddy-shedding" or onshore-turning events occur about ten times. Figure 16 plots longitude-time contours of vorticity (right two panels) along Lines C and D (please see Figures 4 or 15) and "eddy" events show up as high-vorticity (red and violet-red) patches around 118^{o}~119^{o}W. Three major events are indicated by the double-arrowed dashed lines connecting the panels. As shown by the V-wind speed contours along Line A (just downwind of Pt. Conception) on the left panel, these events are clearly linked to strong equatorward wind events with speeds exceeding 10 m s^{-1} (blue). The cyclonic eddies are similar to those sometimes observed, the so called "Catalina Eddies" (Rosenthal, 1968; Bozart, 1983; Dorman, 1985a; Wakimoto, 1987; Mass and Albright, 1989; Clark and Dembek, 1991; Ueyoshi and Roads, 1993; Clark, 1994), but as cautioned by Dorman and Winant (2000) different events may be associated with different causes and dynamics.

6. SUMMARY AND CONCLUSIONS

Accurate wind information is required in order to accurately calculate ocean currents. This is particularly true in the Santa Barbara Channel region, where a combination of complex orography and generally equatorward wind means cool upwelled ocean water near the surface and thin marine (atmospheric) boundary layer, the dynamics of which are uncoupled from those of winds higher up (Burk and Thompson, 1996; Dorman et al., 1999, 2000). Both wind stress and wind stress curl, and their variations, are important because they force and in part determine the internal pressure distribution of the ocean. In this paper, we apply COAMPS to simulate winds, with the objective of using them in ocean hindcast experiments in the SBC region. Here we check COAMPS simulated winds against observations for the period March-May 1999. This is a spring transition period when the wind changes from its characteristics more typical of winter (storm passages) in early March, through April when intense equatorward wind bursts sweep over the region, and into May when more persistent and intense equatorward winds off central California coast sets up a supercritical expansion fan over the western portion of the channel, compression jump ensues in the central channel, and weak winds in the east. The complexity of the wind field poses a challenge to any model.

We compare COAMPS with wind time-series from NDBC, coastal and island wind stations in the vicinity of the channel. While the agreement is good during March and April, it is poor in May especially for the eastern stations. At grid sizes $\Delta = 9$ km, the model fails to accurately resolve the compression jump and the much weakened wind field to the east. Instead, the modeled winds east and west are part of the same large-scale system over the open ocean, rather than uncorrelated as observed. On the other hand, the results from $\Delta = 9$ km are superior than those from $\Delta = 27$ km, which suggests that the model skill should improve with even finer grid size, $\Delta = 3$ km, say.

On a larger scale, COAMPS simulated wind speeds over the open ocean are in good agreement with those obtained from satellite (SSM/I). Over the Southern California Bight and the near-coast zone in particular, COAMPS correctly simulates onshore cyclonic turning of the wind in agreement with observed climatology. This contrasts coarser-grid ECMWF reanalysis wind product (on 1.125^o Gaussian grid), which gives little turning. COAMPS simulation indicates that the onshore turning is in part driven by cyclonic “eddies” or vorticity shed downwind of Pt. Conception. The shedding appears to be preceded by a period (days) of intense equatorward wind off the central California coast and open ocean, though the exact mechanism has yet to be uncovered. Southward along the coast in Southern California Bight, COAMPS wind stress curl continuously weakens, a feature that has important consequences in driving the observed poleward surface current in the ocean (please see Oey, 1996, 1999, and references quoted therein).

ACKNOWLEDGMENTS

We thank Walt Johnson (MMS) for making the ECMWF data available to us, and also Ed Dever and Lynn Yarmey (SIO) for preparing and providing us with the OI-mapped wind data in the Santa Barbara Channel. Carrie Zhang processed the SSM/I data. This work was funded by the Office of Naval Research and the Minerals Management Service. Computing was performed at the Geophysical Fluid Dynamic Laboratory, Princeton.

REFERENCES

Allen, J.S., 1980: Models of wind-driven currents on the continental shelf. *Ann. Rev. Fluid Mech., 12,* 389-433.

Beardsley, R.C. and S.J. Lentz, 1987: The Coastal Ocean Dynamics Experiment collection: An Introduction. *J. Geophys. Res.,* **92,** 1455-1463.

Bosart, L.F., 1983: Analysis of a California Catalina eddy event. *Mon. Wea. Rev.,* **111,** 1619—1633.

Brink, K.H. and R.D. Muench, 1986: Circulation in the Point Conception-Santa Barbara Channel region. *J. Geophys. Res.,* **91,** 877-895.

Burk, S.D., and W.T. Thompson, 1996: The summertime low—level jet and marine boundary layer structure along the California coast. *Mon. Wea. Rev.,* **124,** 668—686.

Burk, S.D., T. Haack, and R.M. Samelson, 1999: Mesoscale simulation of supercritical, subcritical, and transcritical flow along coastal topography. *J. Atmos. Sci.,* **56**, 2780—2795.

Caldwell, P.C., D.W. Suart, and K.H. Brink, 1986: Mesoscale wind variability near Point Conception, California during spring 1983. *J. Climate Appl. Meteor.,* **25,** 1241-1254.

Clark, J.H.E., 1994: The role of Kelvin waves in evolution of the Catalina eddy. *Mon. Wea. Rev.,* **122,** 838—850.

Clark, J.H.E., and S.R. Dembek, 1991: The Catalina eddy event of July 1987: A coastally trapped mesoscale response to synoptic forcing. *Mon. Wea. Rev.,* **119,** 1714—1735.

Davis, R.E., 1976: Predictability of sea surface temperature and sea level pressure anomalies over the North Pacific Ocean, *J. Phys. Oceanogr., 3,* 249-266.

Dorman, C.E., 1985a: Evidence of Kelvin waves in California's marine layer and related eddy generation. *Mon. Wea. Rev.,* **113,** 827-839.

Dorman, C.E., 1985b: Hydraulic control of the northern California marine layer. *EOS, Trans. Amer. Geophys. Union,* **66,** 914.

Dorman, C.E., D.P. Rogers, W.Nuss, W.T. Thompson, 1999: Adjustment of the summer marine boundary layer around Point Sur, Californoa. *Mon. Wea. Rev.,* **127,** 2143—2159.

Dorman, C.E., T. Holt, D.P. Rogers, K. Edwards, 2000: Large-scale structure of the June-July 1996 marine boundary layer along California and Oregon. *Mon. Wea. Rev.,* **128,** 1632-1652.

Dorman, C.E., and C.D. Winant, 1995: Buoy observations of the atmosphere along the west coast of the United States, 1981—1990. *J. Geophys. Res.,* **100,** 16029—16044.

Dorman, C.E., and C.D. Winant, 2000: The structure and variability of the marine atmosphere around the Santa Barbara Channel. *Mon. Wea. Rev.,* **128,** 261—282.

Doyle, J.D., 1997: The influence of mesoscale topography on a coastal jet and rainband. *Mon. Wea. Rev.,* **125,** 1465—1488.

Haack, T., S.D. Burk, C.E. Dorman, and D.P. Rogers, 2001: Supercritical flow interaction within the Cape Blanco—Cape Mendocino orographic complex. *Mon. Wea. Rev.,* **129,** 688—708.

Harms, S. and Winant, C.D. 1998: Characteristic patterns of the circulation in the Santa Barbara Channel. *JGR-Oceans*, 103: 3041-3065.

Hodur, R., 1997: The Naval Research Laboratory's Coupled Ocean/Atmosphere Mesoscale Prediction System (COAMPS). *Mon. Wea. Rev.,* **125,** 1414—1430.

Harshvardhan, D. Randall, and T. Corsetti, 1987: A fast radiation parameterization for atmospheric circulation models. *J. Geophys. Res.,* **92,** 1009—1016.

Kain, J.S., and J.M. Fritsch, 1990: A one—dimensional entraining/detraining plume model and its application in convective parameterization. *J. Atmos. Sci.,* **47**, 2784—2802.

Koračin, D., and C.E. Dorman, 2001: Marine atmospheric boundary layer divergence and clouds along California in June 1996. *Mon. Wea. Rev.,* **129,** 2040—2056.

Large, W.G. and S. Pond, 1981: Open ocean momentum flux measurements in moderate to strong winds, *J. Phys. Oceanogr., 11,* 324-336.

Mass, C.F. and M.D. Albright, 1989: Origin of the Catalina eddy. *Mon. Wea. Rev.,* **117,** 2406—2436

Munchow, A. 2000: Wind stress curl forcing of the coastal ocean near Point Conception, California. *J. Phys. Oceanogr.*, 30, 1265-1280.

Oey, L.-Y. 1996: Flow around a coastal bend: a model of the Santa Barbara Channel eddy. *JGR-Oceans*, 101, 16,667-16,682.

Oey, L.-Y. 1999. A Forcing Mechanism for the Poleward Flow off the Southern California

Coast, *JGR-Oceans*, 104, 13,529-13,539.

Oey, L.-Y. 2000: Understanding and predicting coastal circulation based on strategically located observation stations. In Proceedings of the 2nd International Ocean & Atmosphere Conference, Taipei, Taiwan, Jul 10-12, 2000, pp.201-216.

Oey, L.-Y., D.-P. Wang, T. Hayward, C. Winant, & M. Hendershott. 2001: Upwelling and cyclonic regimes of the near-surface circulation in the Santa Barbara Channel. *JGR-Oceans*, 106, 9213-9222.

Oey, L.-Y., C. Winant, E. Dever, W. Johnson, and D.-P Wang, 2002: A data-assimilated model of the near-surface circulation of the Santa Barbara Channel: comparison with observations and dynamical interpretations. Submitted, *J. Phys. Oceanogr.*

Rothenthal, J., 1968: A Catalina eddy. *Mon. Wea. Rev.,* **96,** 742—743.

Rutledge, S. A., and P.V. Hobbs, 1983: The mesoscale and microscale structure of organization of clouds and precipitation in midlatitude cyclones. VIII: A model for the “seeder—feeder” process in warm—frontal rainbands. *J. Atmos. Sci.,* **40**, 1185—1206.

Samelson, R., 1992: Supercritical marine-layer flow along a smoothly varying coastline. *J. Atmos. Sci.,* **49,** 1571-1584.

Samelson, R., P. Barbour, J. Barth, S. Bielli, T. Boyd, D. Chelton, P. Kosro, M. Levine, E. Skyllingstad, and J. Wilczak, 2002: Wind stress forcing of the Oregon coastal ocean during the 1999 upwelling season. *J. Geophys. Res.,* **107,** C5, 10.1029/2001JC000900.

Therry, G., and P. LaCarrere, 1983: Improving the eddy kinetic energy model for planetary boundary layer description. *Bound.—Layer Meteor*., **25**, 63—88.

Thompson, W.T., S.D. Burk, J. Rosenthal, 1997: An investigation of the Catalina eddy. *Mon. Wea. Rev.,* **125,** 1135—1146.

Ueyoshi, K., and J.O. Roads, 1993: Simulation and prediction of the Catalina eddy. *Mon. Wea. Rev.,* **121,** 2975—3000.

Wakimoto, R., 1987: The Catalina eddy and its effect on pollution of Southern California. *Mon. Wea. Rev.,* **115,** 837—855.

Wang, D.-P., 1997: Effects of small-scale wind on coastal upwelling with application to Point Conception. *JGR-Oceans*, 102, 15,555-15,566.

Wentz F. J. 1997, "A well-calibrated ocean algorithm for SSM/I", J. Geophys. Res., Vol. 102, No. C4, pg. 8703-8718.

Wentz, Frank J. and Roy W. Spencer, May 1, 1998, "SSM/I Rain Retrievals within a Unified All-Weather Ocean Algorithm", Journal of the Atmospheric Sciences, Vol. 55, pg. 1613-1627.

Winant, C., R. Beardsley, C. Dorman, and C. Friehe, 1988: The marine layer off northern California: an example of supercritical channel flow. *J. Atmos. Sci.,* **45**, 3588-3605.

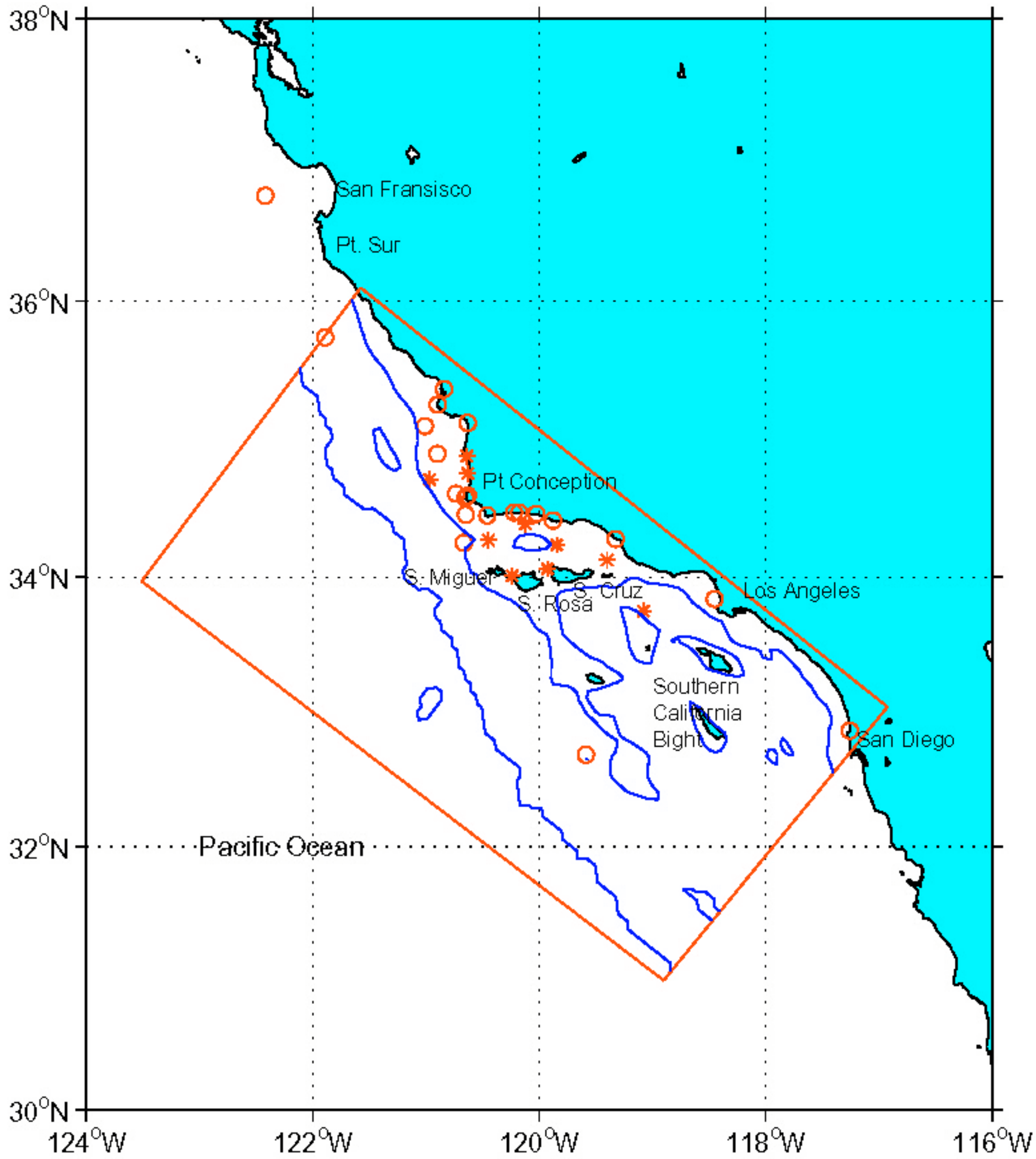

Figure 1. A locator map of the ocean region of interest, off the California coast, including the Santa Barbara Channel and Southern California Bight. The rectangle is the ocean model domain used by Oey (1996) and Oey et al. (2001) and contours show the 500 m and 2000 m isobaths. Open circles and asterisks denote wind stations where we have analyzed the wind data. The asterisks denote those presented in details in the text.

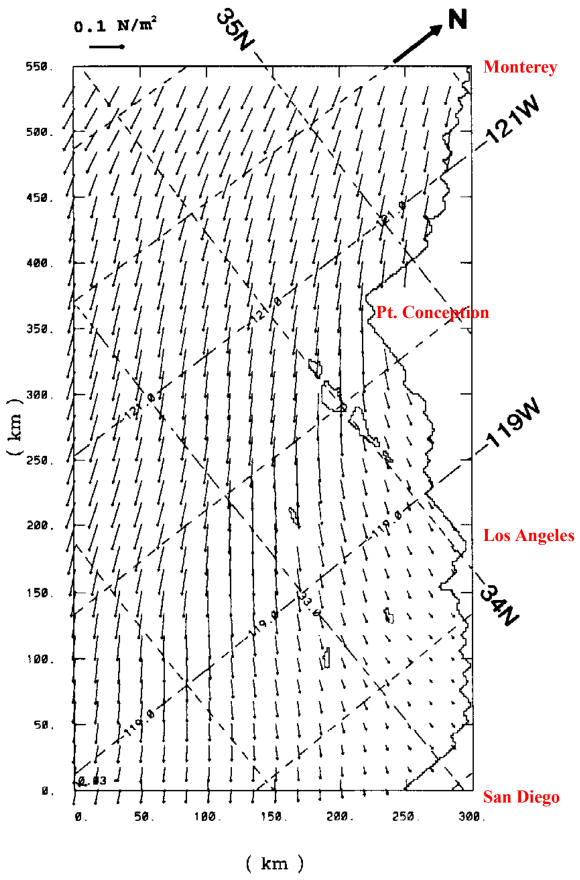

Spring (MAM) Wind Stress

Figure 2. California Cooperative Oceanic Fisheries Investigation (CalCOFI) spring (March/April/May) wind stress over central California shelf/slope and southern California Bight. Maximum vector is 0.16 N m^{-2}. (From Oey, 1996).

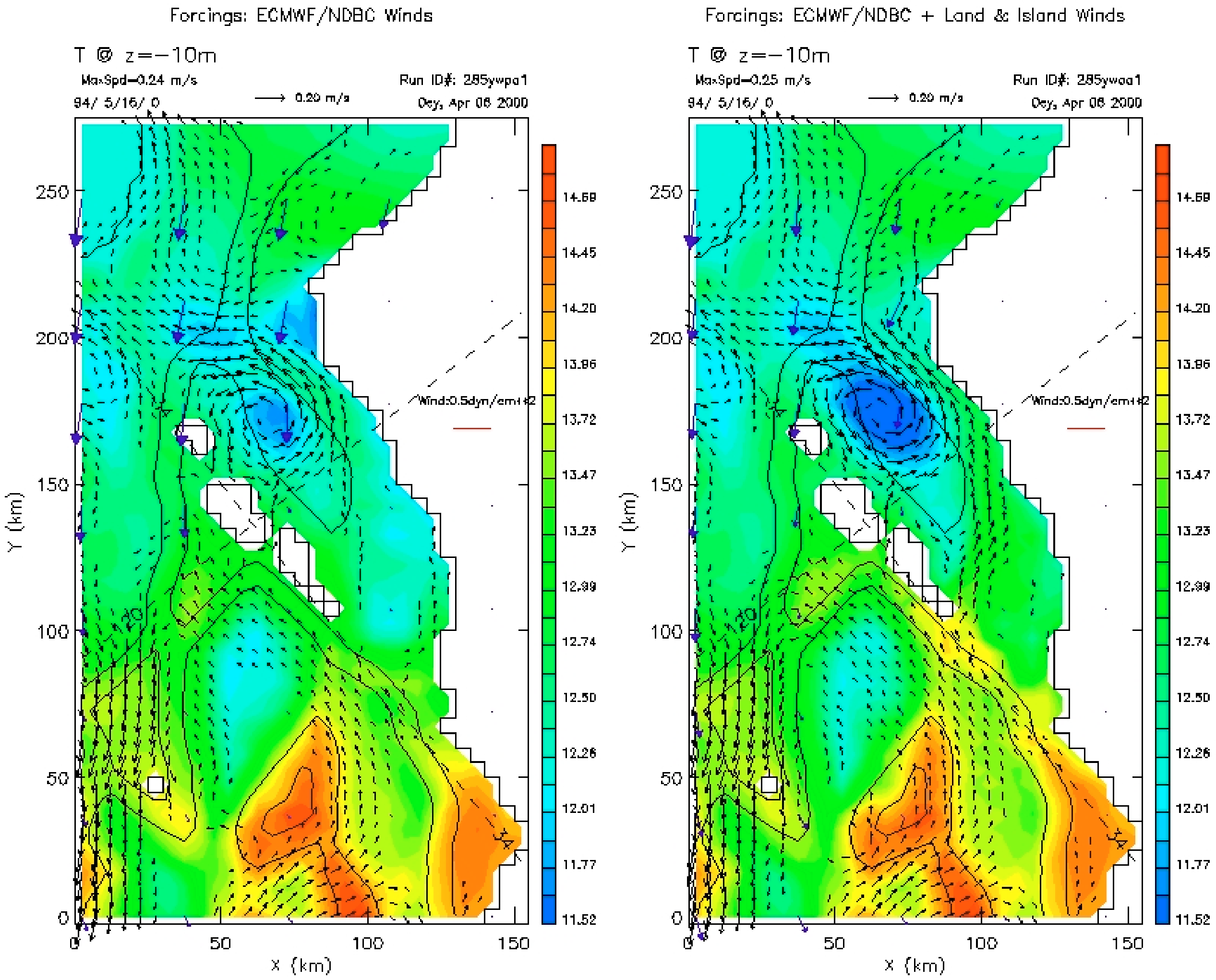

Figure 3a. Averaged (May/06-16/1994) modeled temperature and velocity vectors (black) at z=-10m below the free surface for the case when ECMWF supplemented by over-ocean (NDBC) buoy winds were used (left panel) and when in addition land and island-based wind data were also utilized (right panel) to force the model. The wind vectors are shown as blue arrows and the corresponding wind stress curl fields are shown in Figure 3b. Solid contours show the 300m, 600m and 2000m isobaths. The Princeton Ocean Model was used with 5km×5km×31 sigma levels – see Oey (1996) and Oey et al. (2000) for model domain, boundary conditions and other details. (From Oey, 2000).

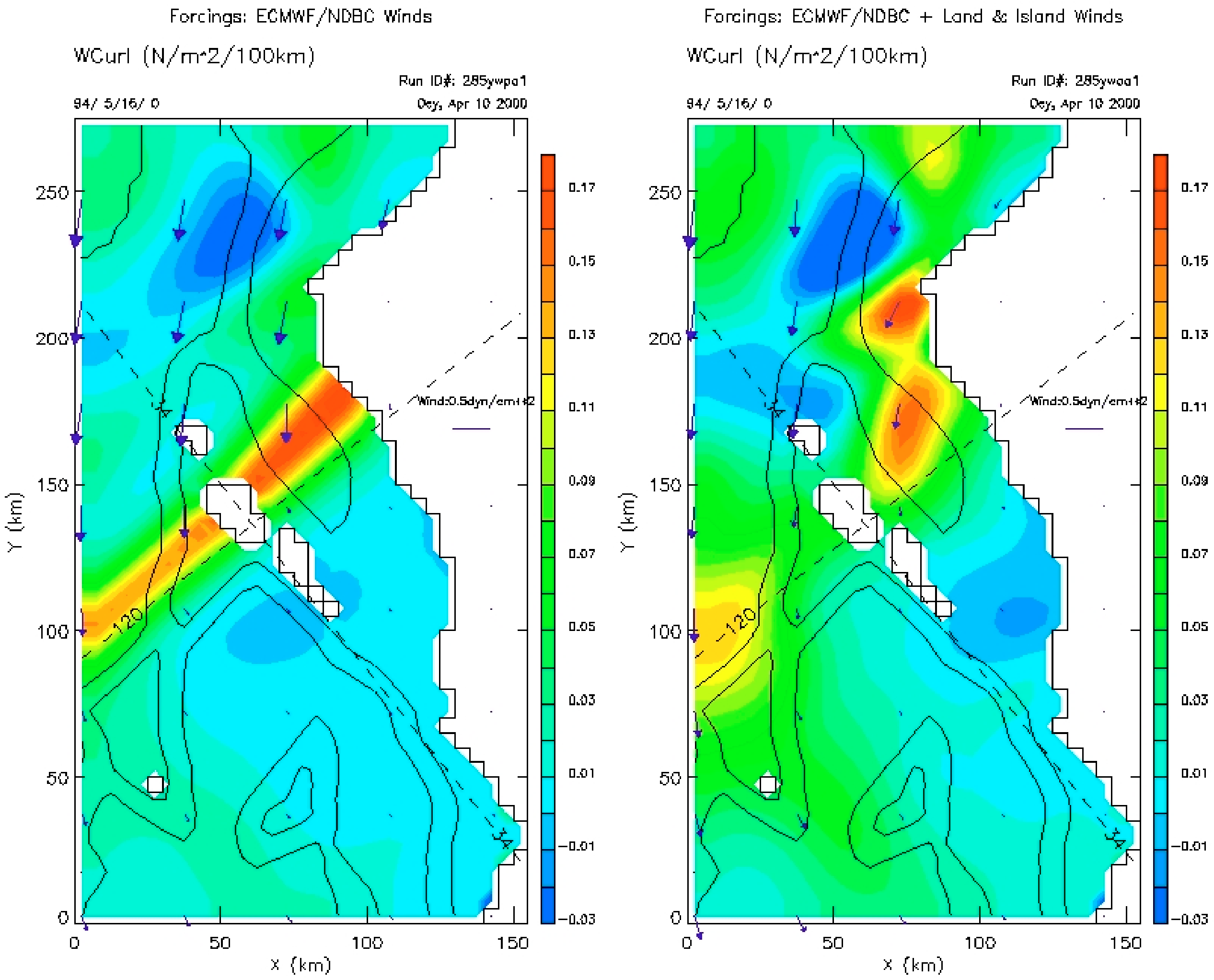

Figure 3b. Averaged (May/06-16/1994) wind stress curl for the case when only over-ocean (NDBC) buoy winds were used in the channel (left panel) and when both over-ocean and land and island-based wind data were used (right panel) to supplement the ECMWF wind. Solid contours show the 300m, 600m and 2000m isobaths. Arrows indicate the corresponding wind stresses. (From Oey, 2000).

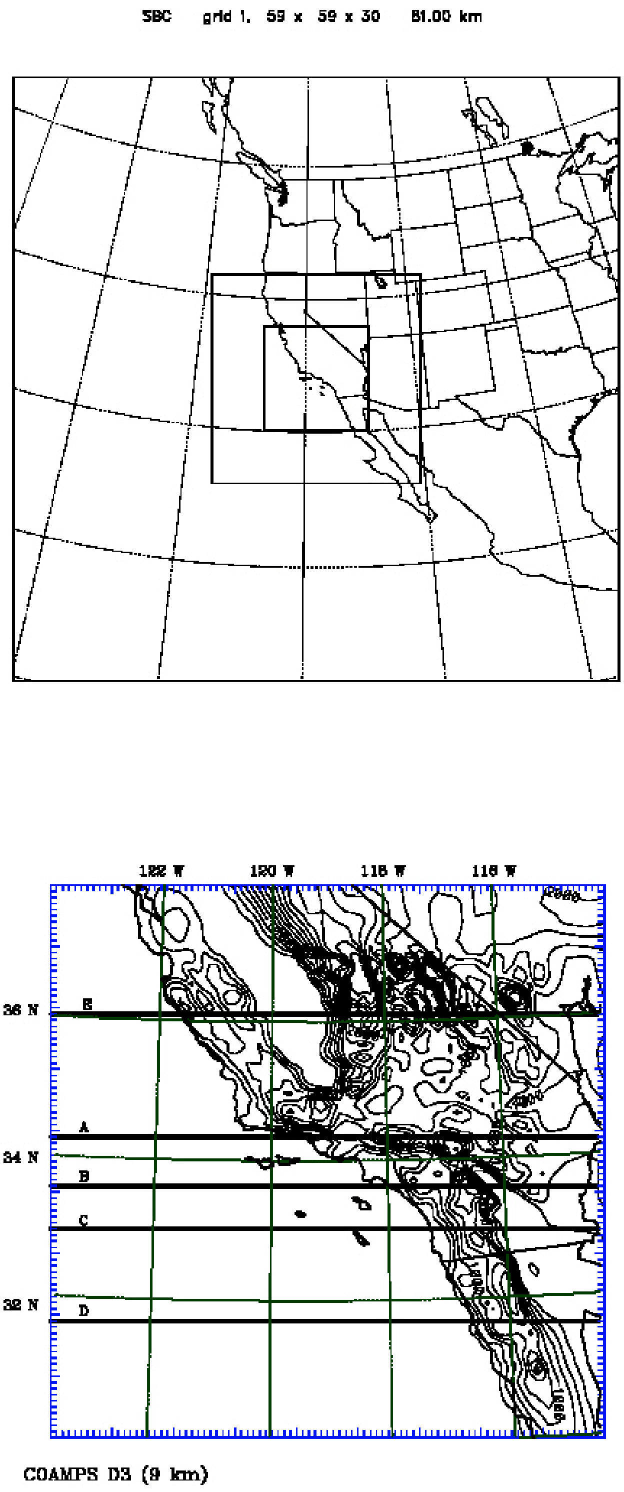

Figure 4. Top panel: the triple-nest configurations of COAMPS used in the present study; outer nest (Domain 1 or D1) has Δ = 81 km, middle nest (Domain 2 or D2) has Δ = 27 km and inner nest (Domain 3 or D3) has Δ = 9 km. Lower panel: Inner nest with detailed land orography (contours from 0 to 3500 m at 250 m interval) and west-to-east transacts where model results are discussed in text.

Figure 5. The three-month averaged (March, April and May, 1999) 10-m fields from COAMPS' inner nest (Δ = 9 km) results, (A) wind speed, (B) wind stress, (C) wind stress curl and (D) wind divergence. In (C) and (D), solid contour curves denote the zero contours. Surface streamlines indicating flow directions are superimposed on each panel.

(A) WIND SPEED **(C) WIND STRESS CURL**

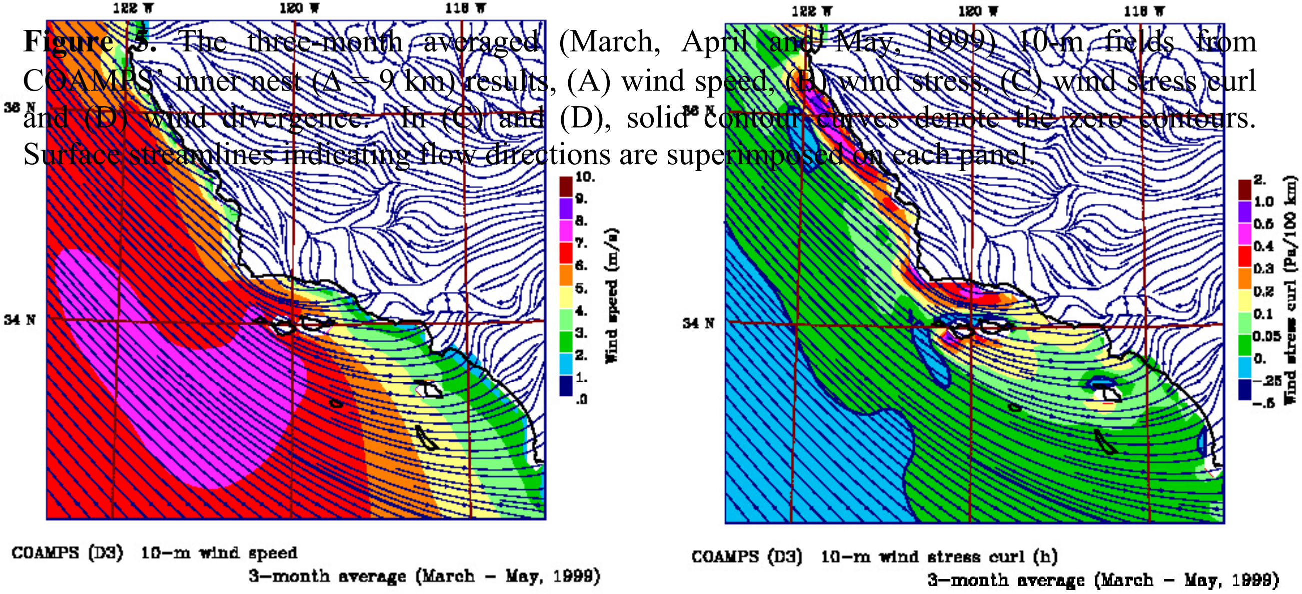

(B) WIND STRESS **(D) WIND DIVERGENCE**

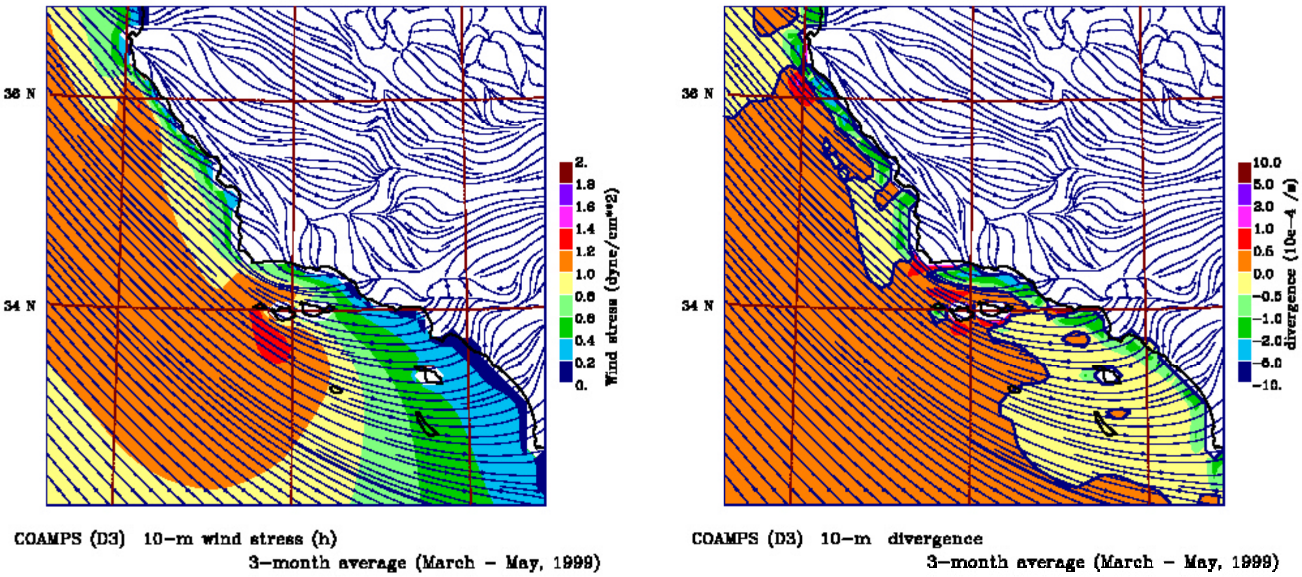

(A) WIND SPEED

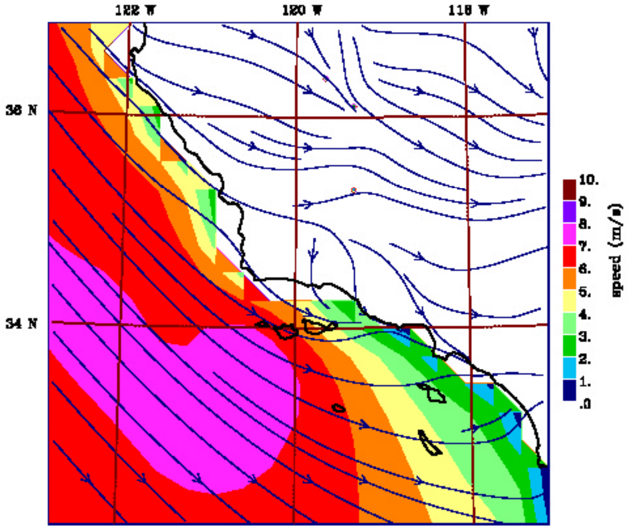

COAMPS (D2) 10–m wind speed
3–month average (March – May, 1999)

(C) WIND STRESS CURL

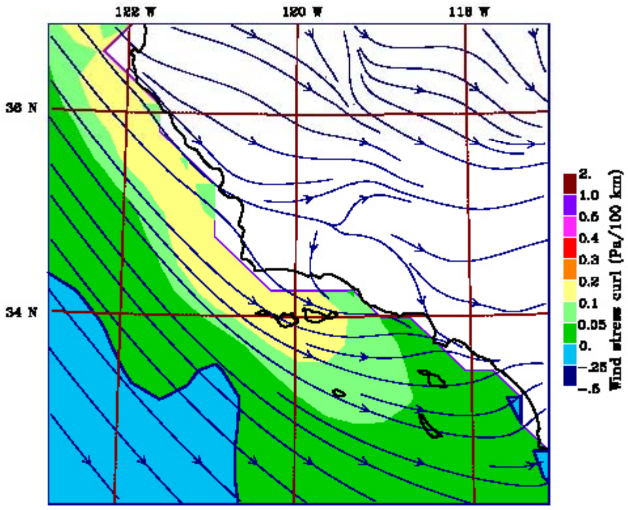

COAMPS (D2) 10–m wind stress curl
3–month average (March – May, 1999)

(B) WIND STRESS

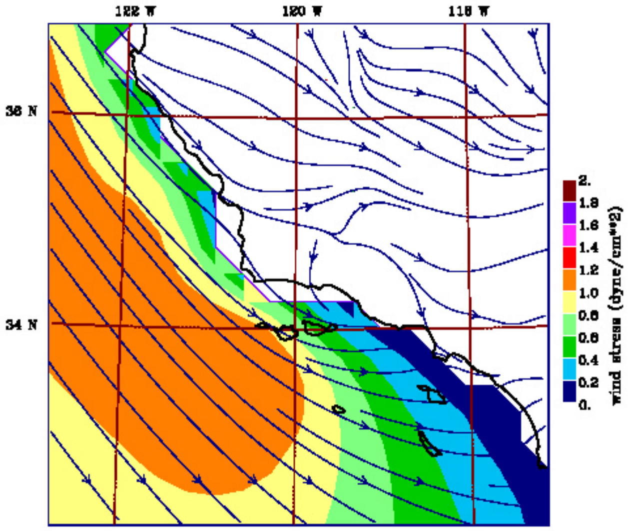

COAMPS (D2) 10–m wind stress
3–month average (March – May, 1999)

(D) WIND DIVERGENCE

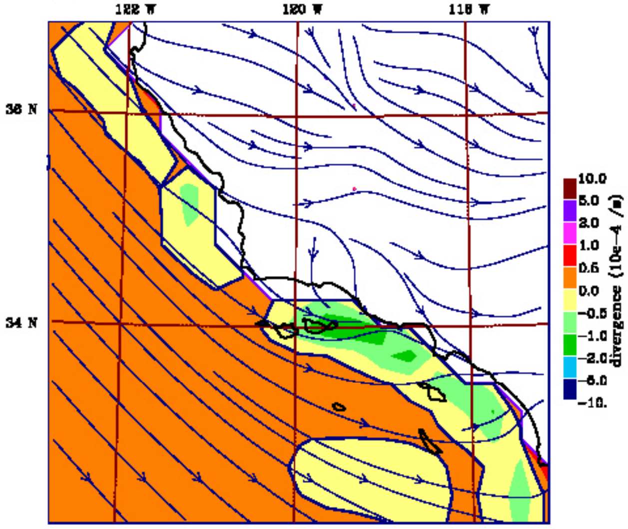

COAMPS (D2) 10–m divergence
3–month average (March – May, 1999)

Figure 6. The three-month averaged (March, April and May, 1999) 10-m fields from COAMPS' middle nest ($\Delta = 27$ km) results, (A) wind speed, (B) wind stress, (C) wind stress curl and (D) wind divergence. In (C) and (D), solid contour curves denote the zero contours. Surface streamlines indicating flow directions are superimposed on each panel.

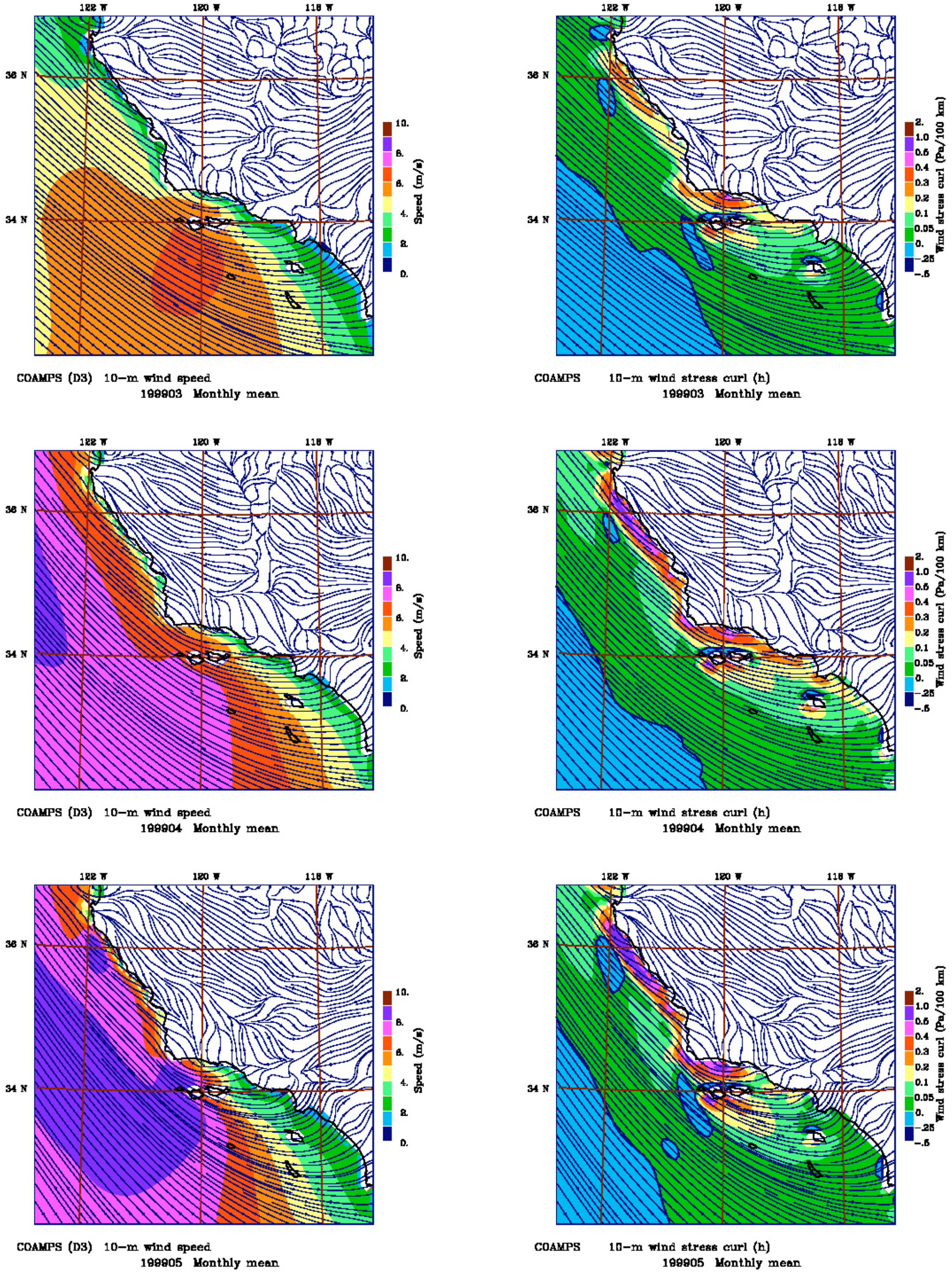

COAMPS (D3) 10–m wind speed
199903 Monthly mean

COAMPS 10–m wind stress curl (h)
199903 Monthly mean

COAMPS (D3) 10–m wind speed
199904 Monthly mean

COAMPS 10–m wind stress curl (h)
199904 Monthly mean

COAMPS (D3) 10–m wind speed
199905 Monthly mean

COAMPS 10–m wind stress curl (h)
199905 Monthly mean

Figure 7. The monthly-mean (March, April and May, 1999) fields: (a) left column: wind stress and (b) right column: wind stress curl. These were derived from COAMPS' inner nest ($\Delta = 9$ km) domain.

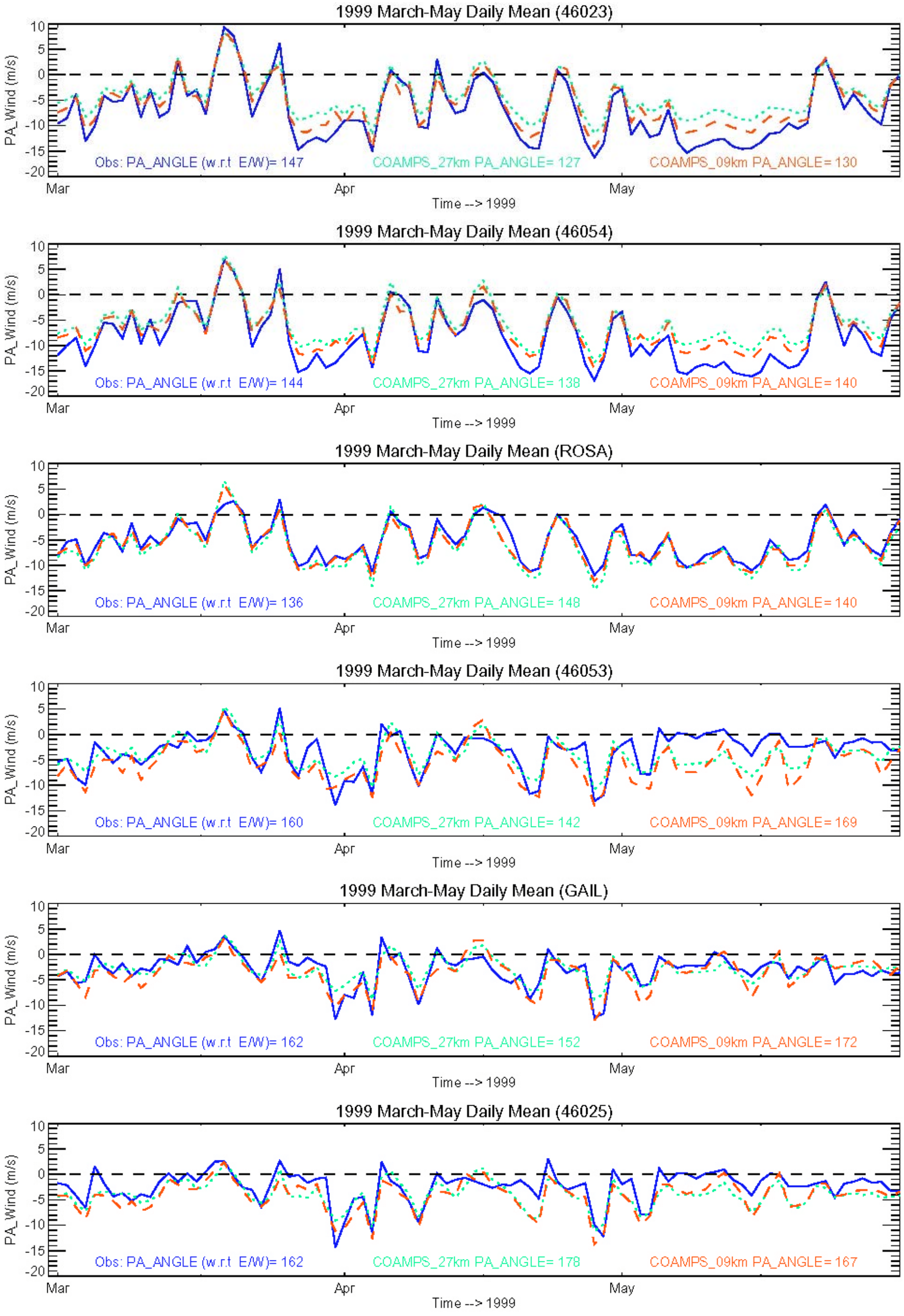

Figure 8. Wind time series from March through May 1999, shown here as daily averaged principal-axis values at six NDBC and coastal stations arranged from north (top panel) to south: 46023, 54, ROSA, 53, GAIL and 25 (please see Figure 1 for locations). The principal-axis angles, measured in degrees anti-clockwise from true east, are printed in each panel. Solid curves are observed, dotted are modeled from the middle nest (Δ = 27 km), and dashed are modeled from the inner nest (Δ = 9 km).

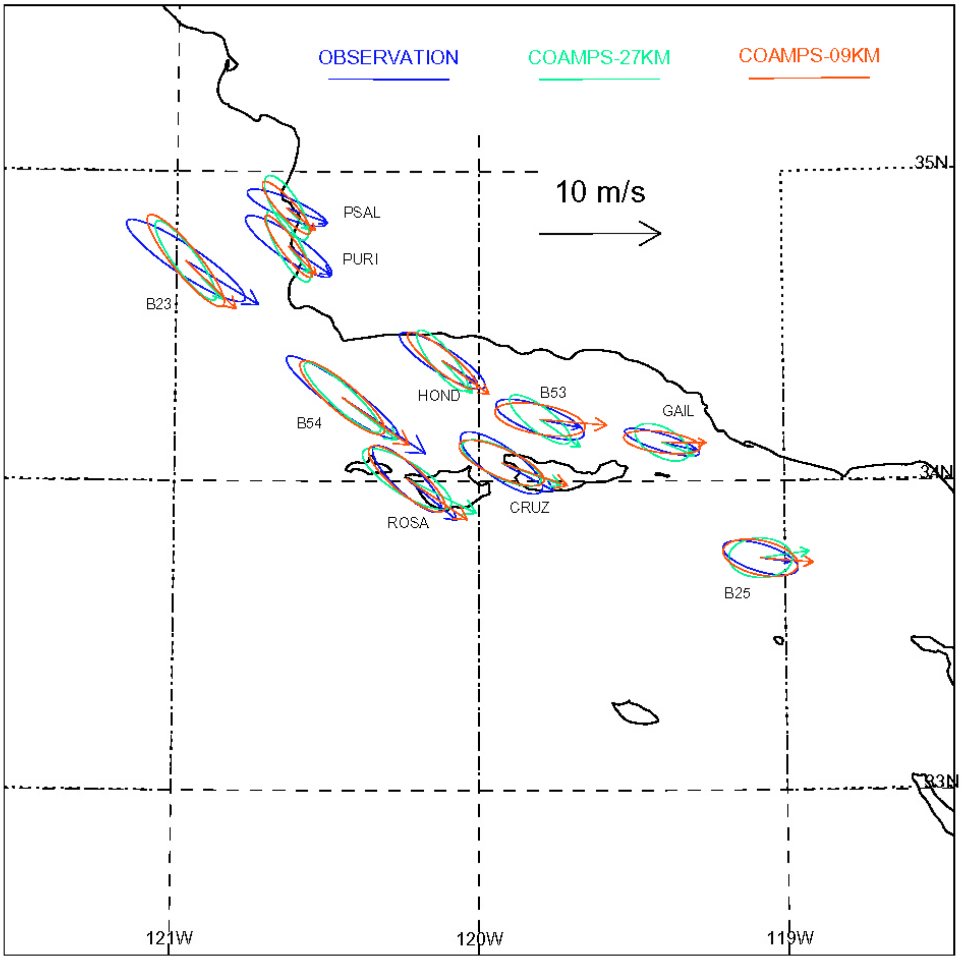

Figure 9. Wind principal-axis ellipses at the ten indicated stations in the vicinity of the Santa Barbara Channel, for period March through May 1999. The wind vectors are also shown. Blue colors are observed, green are modeled from the middle nest (Δ = 27 km), and red are modeled from the inner nest (Δ = 9 km).

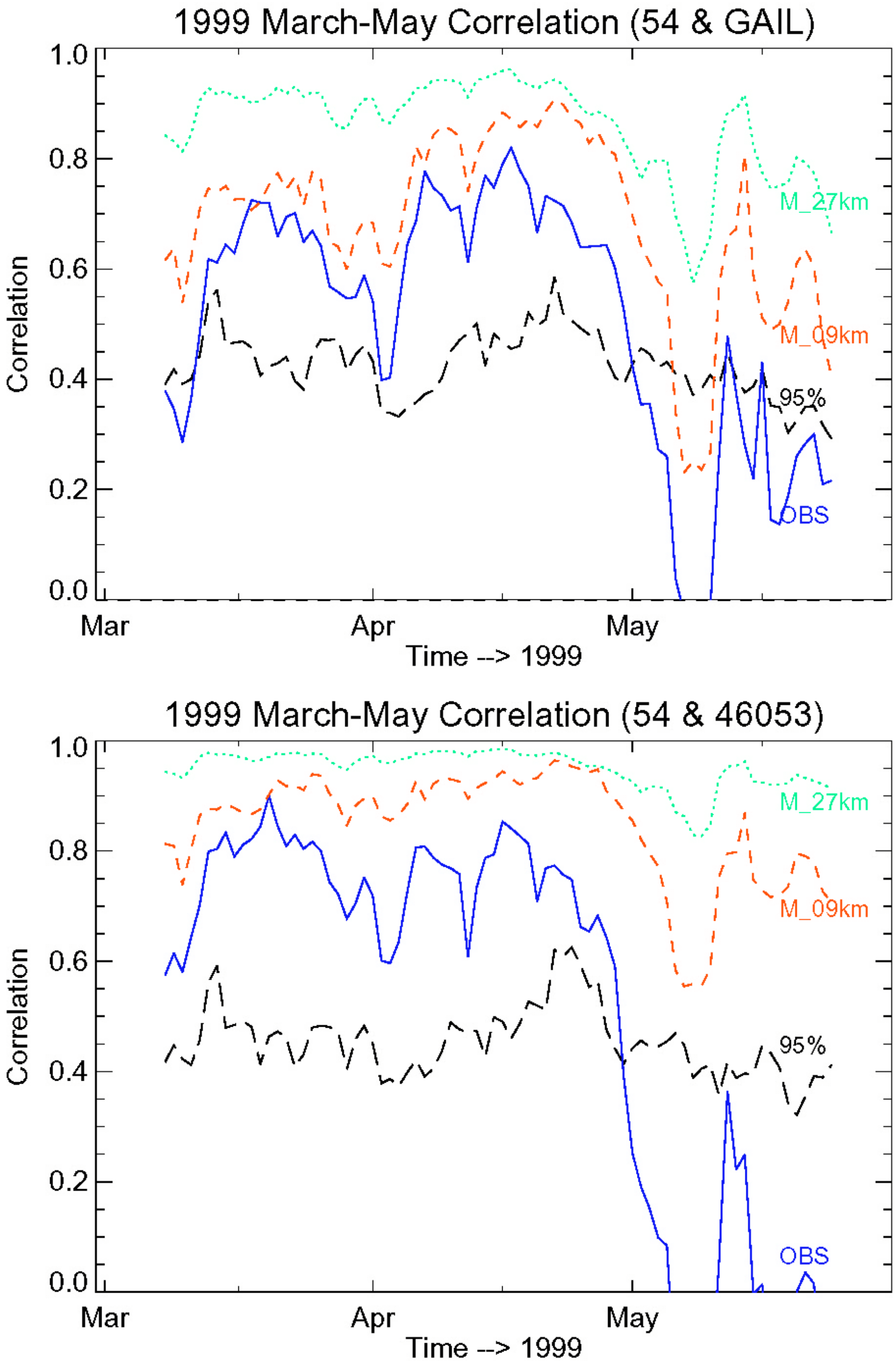

Figure 10. Correlations between B54 and GAIL (top panel) and B54 and B53 (bottom panel) during March through May 1999. Solid curves are observed, dotted are modeled from the middle nest (Δ = 27 km), and dashed are modeled from the inner nest (Δ = 9 km). The 95% significance level curve is also plotted. The correlation was computed using a fifteen-day moving window.

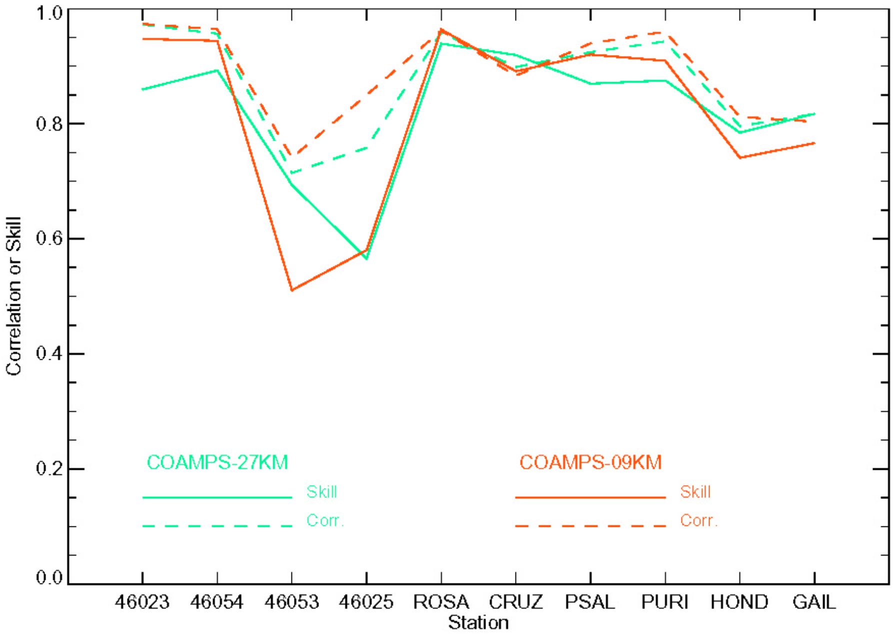

Figure 11. Correlations (dash) between the observed and modeled principal-axis winds at the indicated ten stations in the vicinity of the Santa Barbara Channel. The corresponding skills (solid) are also shown. Green are modeled from the middle nest (Δ = 27 km), and red are modeled from the inner nest (Δ = 9 km).

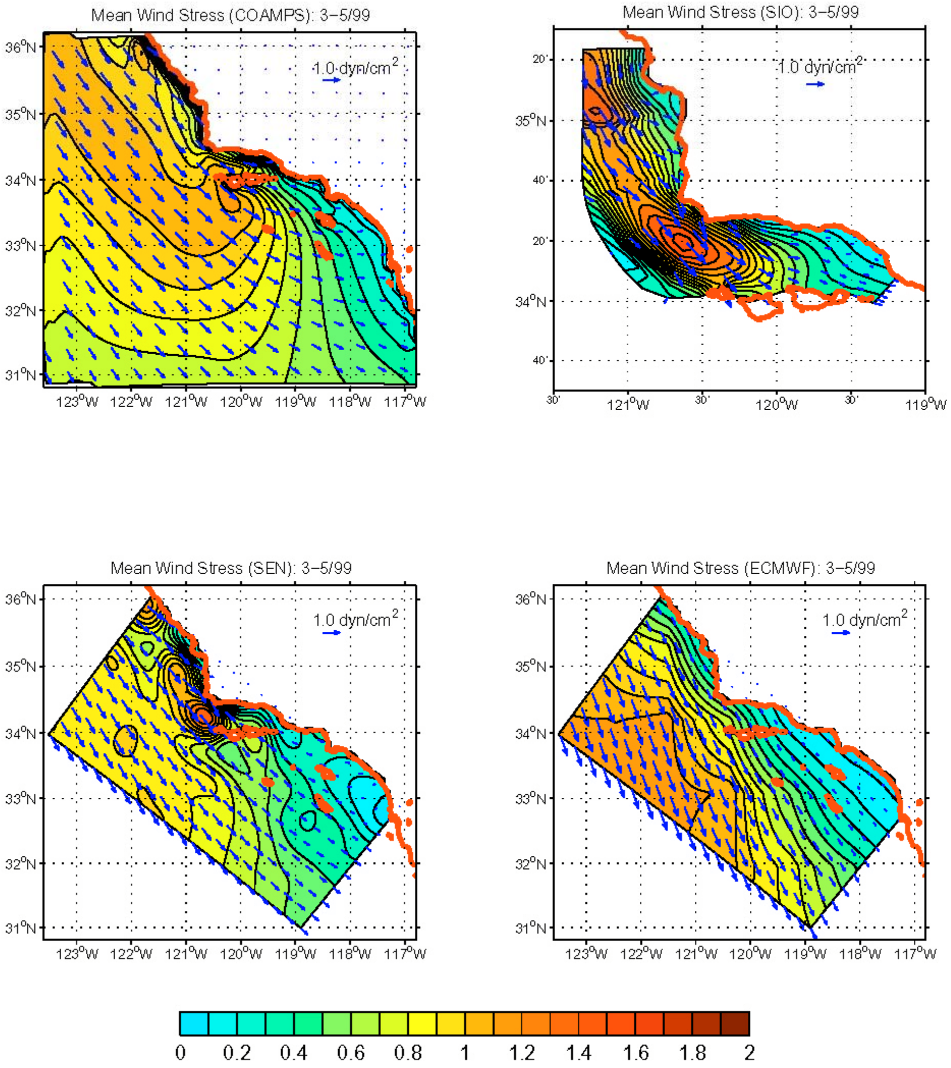

Mean Wind Stress (COAMPS): 3–5/99

Mean Wind Stress (SIO): 3–5/99

Mean Wind Stress (SEN): 3–5/99

Mean Wind Stress (ECMWF): 3–5/99

Figure 12. Three-month (March-May/1999) mean wind stress obtained from COAMPS (upper left; results from the inner nest $\Delta = 9$ km), coastal wind stations (upper right), combined satellite (SSM/I) and wind station data (lower left), and ECMWF 1.125° Gaussian grid reanalysis wind (lower right).

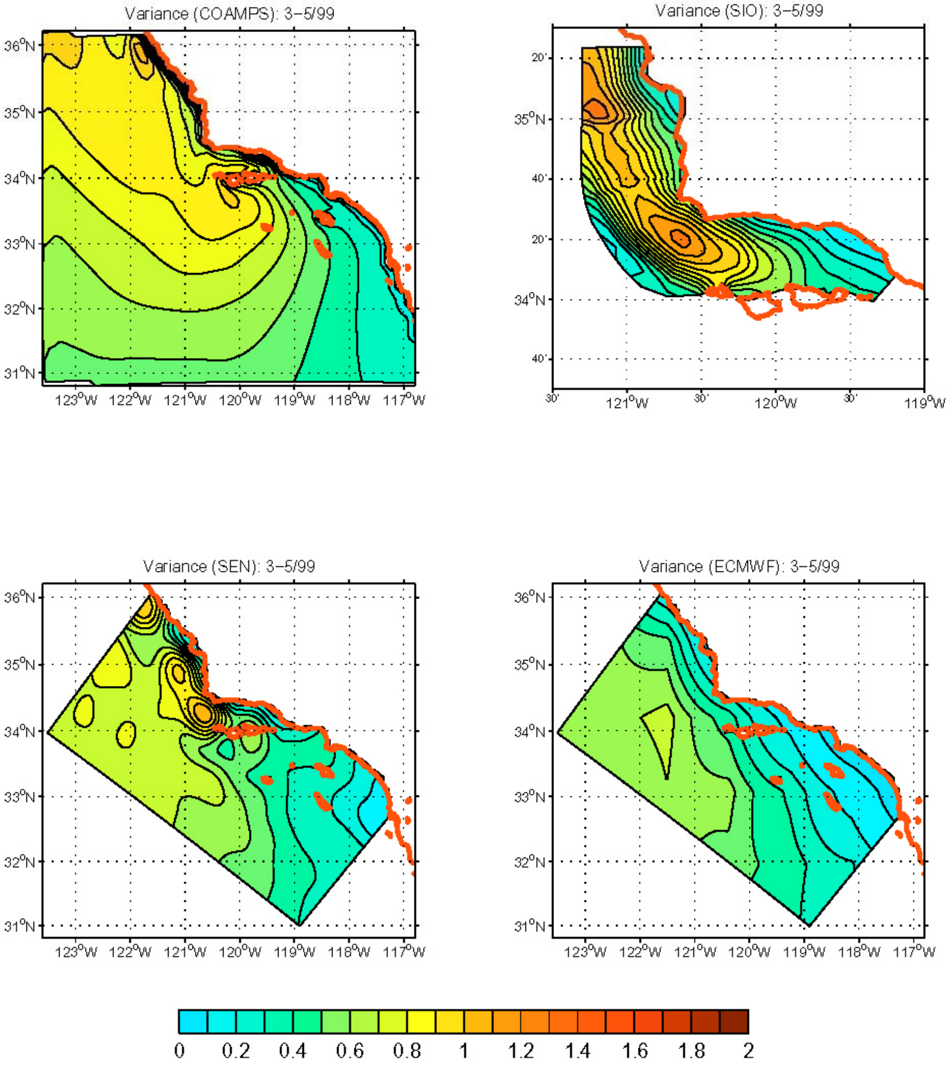

Figure 13. Three-month (March-May/1999) standard deviation of wind stress (dyn/cm^2) obtained from COAMPS (upper left; results from the inner nest Δ = 9 km), coastal wind stations (upper right), combined satellite (SSM/I) and wind station data (lower left), and ECMWF 1.125^o Gaussian grid reanalysis wind (lower right).

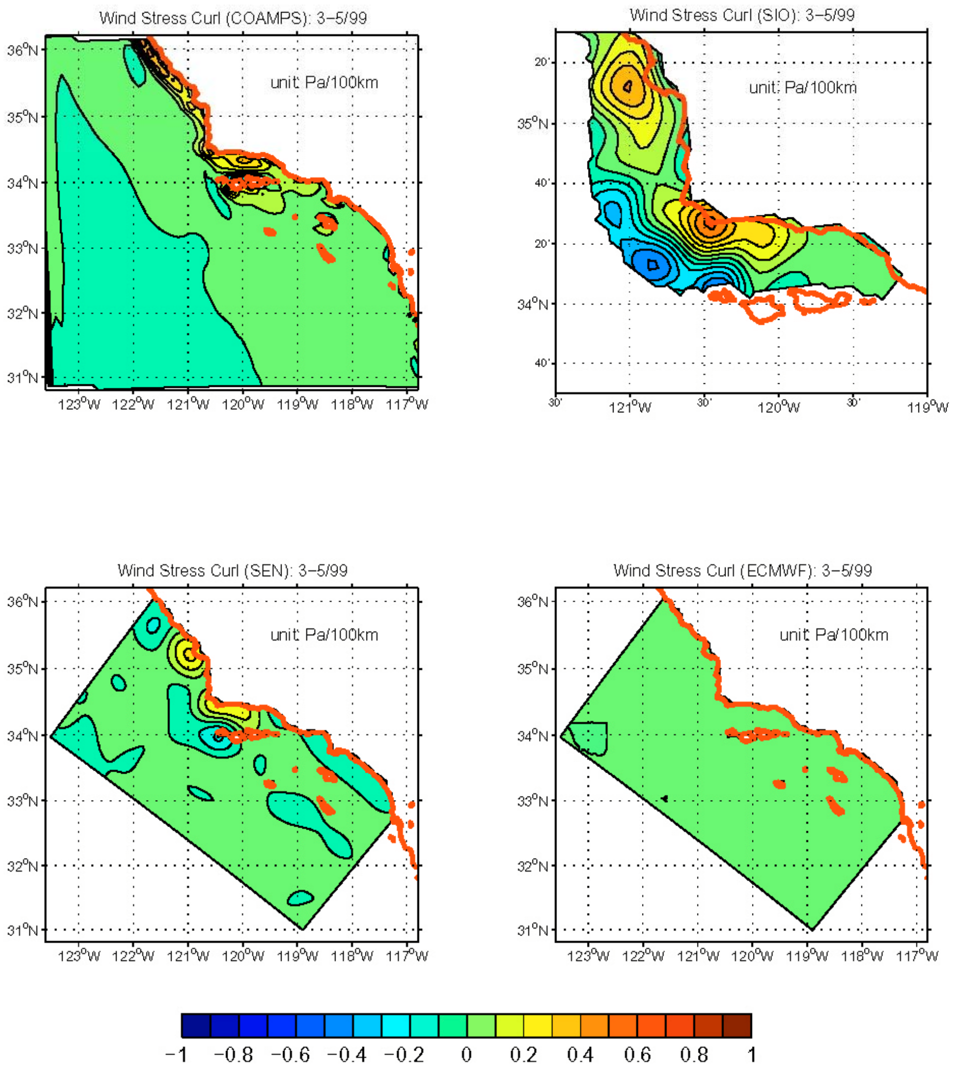

Figure 14. Three-month (March-May/1999) mean wind stress curl (Pa/100 km) obtained from COAMPS (upper left; results from the inner nest $\Delta = 9$ km), coastal wind stations (upper right), combined satellite (SSM/I) and wind station data (lower left), and ECMWF 1.125^{o} Gaussian grid reanalysis wind (lower right).

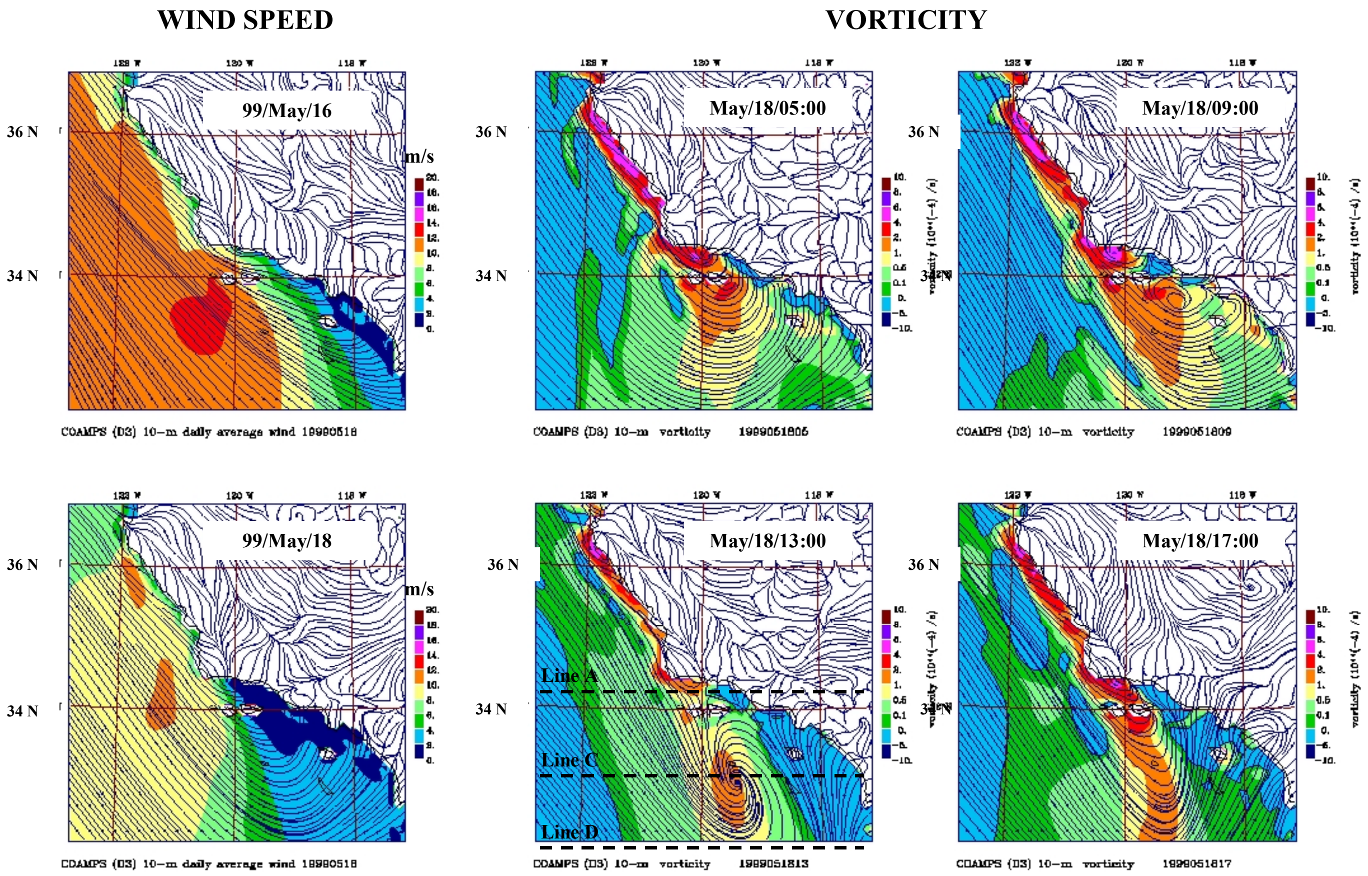

Figure 15. Left column: modeled (inner-nest with Δ = 9 km) wind speed on May/16th and 18th, 1999, showing strong equatorward wind on May/16th. Right four panels: four-hourly modeled vorticity at the indicated time on May/18th/1999, showing the development of a cyclonic eddy downwind of Pt. Conception. Longitude/time contours are plotted in Figure 16 along the three lines A, C and D indicated on May/18/13:00 vorticity panel.

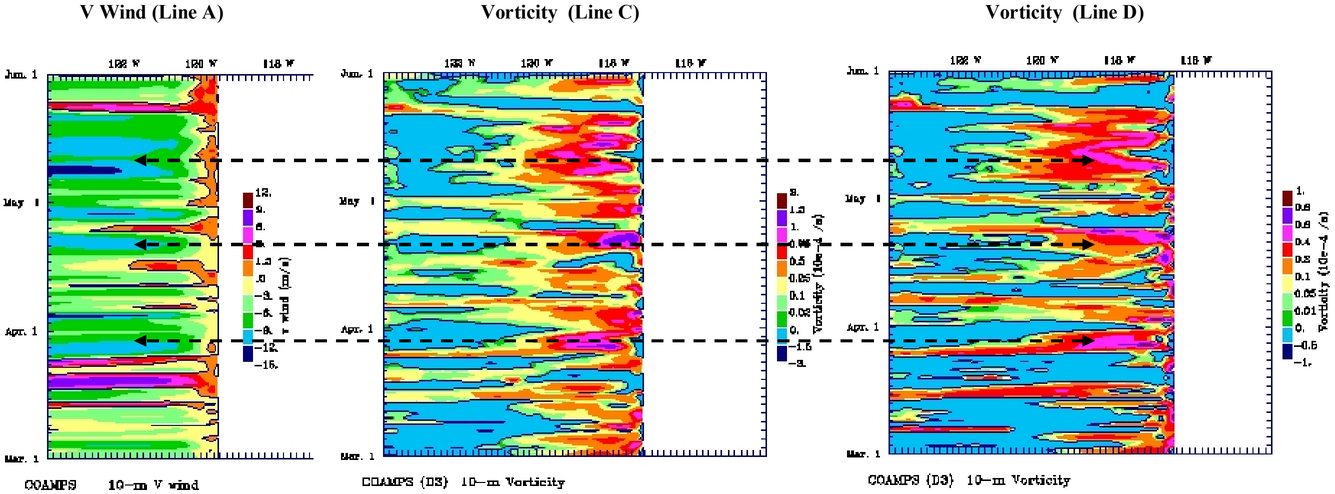
V Wind (Line A)

Vorticity (Line C)

Vorticity (Line D)

Figure 16. Longitude-time contours of: left panel - modeled (inner-nest with Δ = 9 km) V-wind speed along line A (please see Figures 4 or 15) for March through May/1999; right two panels – modeled vorticity along lines C and D respectively. The three doubled-arrowed dashed lines connecting the three panels indicate periods when major (strong) equatorward wind (light-blue) develops off Pt. Conception, and cyclonic eddies are shed downwind and seen in the high positive vorticity (violet-red) at Lines C and D. Maps of the last of these three major eddy events is shown previously in Figure 15.